


Article

Removal of Chromium (VI) from the Steel Mill Effluents Using the Chemically Modified Leaves of *Pteris vittata* as Adsorbent

Qaiser Khan ¹, Muhammad Zahoor ^{2,*}, Syed Muhammad Salman ¹, Muhammad Wahab ¹, Muhammad Talha ² and Abdul Waheed Kamran ³

¹ Department of Chemistry, Islamia College University, Peshawar 25000, Khyber Pakhtunkhwa, Pakistan

² Department of Biochemistry, University of Malakand, Chakdara Dir Lower 18800, Khyber Pakhtunkhwa, Pakistan

³ Department of Chemistry, University of Malakand, Chakdara Dir Lower 18800, Khyber Pakhtunkhwa, Pakistan

* Correspondence: mohammadzahoorus@yahoo.com

Abstract: Chromium (Cr), a metal that is released in appreciable amounts from the steel industry into water bodies, is not only the main causative agent of lung cancer in human but also negatively affects the metabolic activities of plants. Keeping in view the hazardous effects of Cr(VI), the present study was aimed to eliminate it from industrial effluents of steel mills installed in Dargai District Malakand, Pakistan, using chemically modified *Pteris vittata* plant leaves as an adsorbent. The instrumental techniques such as FTIR, surface area analysis, SEM, TGA and EDX were used to evaluate surface functionality, morphology, thermal stability and elemental composition of the modified leaves. To identify the ideal conditions for the biosorption process, batch adsorption tests were carried out under varied conditions of pH, contact time, initial metal concentration, biosorbent dose, as well as temperature. Various models, such as those of Freundlich, Jovanovich, Temkin, Langmuir, and Harkins–Jura, were utilized to explain the isothermal experimental data. The high value of R^2 (0.991) was exhibited by the Langmuir model. Pseudo-first-order, power function, pseudo-second-order, intraparticle diffusion, and Natarajan–Khalaf models were employed to obtain an insight into kinetics of the process. The highest R^2 value, close to unity was recorded with pseudo-second order. At pH = 2, the best elimination of Cr was observed with maximum uptake capacity q_{max} (66.6 mg/g) as calculated from the Langmuir isotherm. The thermodynamic analysis, which was conducted at different temperatures, showed that the nature of this sorption process was exothermic and spontaneous. The modified leaves-based biosorbent could be used as an alternative adsorbent for effective Cr elimination from water, and its use could be extended to other heavy metals and organic pollutants as well, and further experimentation are needed in this regard.

Keywords: chromium; steel mills; isotherms; kinetics



Citation: Khan, Q.; Zahoor, M.; Salman, S.M.; Wahab, M.; Talha, M.; Kamran, A.W. Removal of Chromium (VI) from the Steel Mill Effluents Using the Chemically Modified Leaves of *Pteris vittata* as Adsorbent. *Water* **2022**, *14*, 2599. <https://doi.org/10.3390/w14172599>

Academic Editor: Massimo Zacchini

Received: 30 July 2022

Accepted: 20 August 2022

Published: 23 August 2022

Publisher's Note: MDPI stays neutral with regard to jurisdictional claims in published maps and institutional affiliations.



Copyright: © 2022 by the authors. Licensee MDPI, Basel, Switzerland. This article is an open access article distributed under the terms and conditions of the Creative Commons Attribution (CC BY) license (<https://creativecommons.org/licenses/by/4.0/>).

1. Introduction

Heavy metal contamination has grown to be a significant issue in the present scenario because of its direct effects on living things, including humans and other animals as well as on plants. They can induce a variety of acute and long-term negative consequences if present in concentrations exceeding permissible limits, such as shortness of breath, coughing, and asthma. They also result in digestive complications such as abdominal pain, vomiting, bleeding and neurological complications [1]. In the heavy metals list, Cr(VI) is considered to be of prime concern due to its toxicity [2]. Most of the chromium as well as its compounds found in sewage come from different industries such as pigment manufacturing, metal processing, water cooling, leather tanning and mining [3]. Cr may exist in various oxidation states, but Cr^{+3} and Cr^{+6} are the most stable. As a strong oxidant, Cr(VI) is utilized mostly in the manufacturing of polymers, pigments, paints, and other dyes. In addition to being utilized in the manufacturing of steel, Cr(VI) is also employed in electroplating, the tanning of leather, and the restoration of wood. Cr(III) is not more

hazardous and immobile than Cr(VI), which is more dangerous and can enter aquatic compartments through soils [4,5]. The permissible Cr concentration in water is 0.05 mg/L. It is more mutagenic and carcinogenic beyond this level [6,7]. As per the World Health Organization guidelines, in drinking water, the acceptable value of Cr(VI) is 0.05 mg/L [8]. Consequently, it is crucial to check the level of Cr in water and to maintain its value in aquatic system within the permissible level.

For this purpose, different types of approaches have been employed to remediate Cr(VI) present in wastewater including ion exchange, electrochemical reduction and photo catalytic reduction [9–11]. However, every approach has its limitations, such as chemical reduction, which requires chemical additives and is accompanied by precipitation, whereas electrochemical reduction produces a substantial volume of sludge [12]. Phytoremediation is another technique, in which plants, due to their intrinsic nature, can eliminate metals from soil and aquatic environment, but this also suffers from drawbacks such as deposition of heavy metals in their tissue as well as their slow rate of growth which limits their uses for the mentioned purposes on large scale [13]. Adsorption has been used as the best strategy since it is inexpensive, eco-sustainable, and has a high rate of elimination [14,15].

Various number of mineral and organic low-cost adsorbents were reported in literature for the removal of pollutants such as raw and modified clays, tea wastes, coal fish, saw dust, activated carbon, hazel nut shell and olive tree pruning [16–19].

The adsorption capabilities of the biomass-based adsorbents can more effectively be utilized if the phytoremediation capability of a given plant is evaluated prior to its conversion into a biosorbent.

Herein, we initially evaluated wild plants growing on the banks steel mills drainage lines and out of the tested plants; the one with high phytoremediation capability was converted into a biosorbent. This idea and plant have not been used before for the reclamation of industrial effluents. The study area is Dargai, Malakand, Pakistan, which is a tax-free zone, and therefore, industrialists prefer to install their manufacturing units there, thus very rapidly deteriorating the natural environment of the area. *Pteris vittata* plant leaves locally available were collected from District Dargai KPK Pakistan, dried, converted into fine powder, chemically modified and employed as an adsorbent for the elimination of Cr (VI) from the effluents. FTIR surface area, SEM, EDX and TGA, were used to characterize the modified leaves.

2. Methods and Materials

2.1. Preparation of Adsorbent

In Dargai Malakand, Pakistan, leaves of *Pteris vittata* were gathered from the bank of steel mills drainage lines, cleaned twice with distilled water and then allowed to dry in the shade before being put in an electric oven, at 50 °C. The crunchy leaves were ground into powder and processed through 44-mesh sieve. The powdered samples were cleaned in distilled water to eliminate impurities and dust, present if any. To dry the samples, they were baked in an oven. The dried samples were stored for subsequent processing in airtight vials.

2.2. Chemical Modification of Biosorbent

About 100 g of the powdered were steeped in 2 L of HNO₃ (Sigma Aldrich, Taufkirchen, Germany) solution for 24 h before being filtered through 41 Whatman filter paper and repeatedly rinsed using distilled water. The HNO₃ treatment was conducted to eliminate metals that had previously been affixed to the biomass feedstock. The sodium hydroxide (0.1 M; Sigma-Aldrich, Taufkirchen, Germany) was utilized to neutralize the unused acid. Before being heated at 100 °C in an electric oven, the neutralized adsorbent was dried at room temperature, and its 50 g was processed after being activated in 1 L of CaCl₂ solution (0.1 M). The CaCl₂ treatment (Sigma-Aldrich, Taufkirchen, Germany) was utilized to insert a specific group into biosorbent, which will improve the process of adsorption. From here

on, it will be abbreviated as CMPVL (chemically modified *Pteris vittata* leaves) whereas its schematically its preparation is shown in Figure 1.

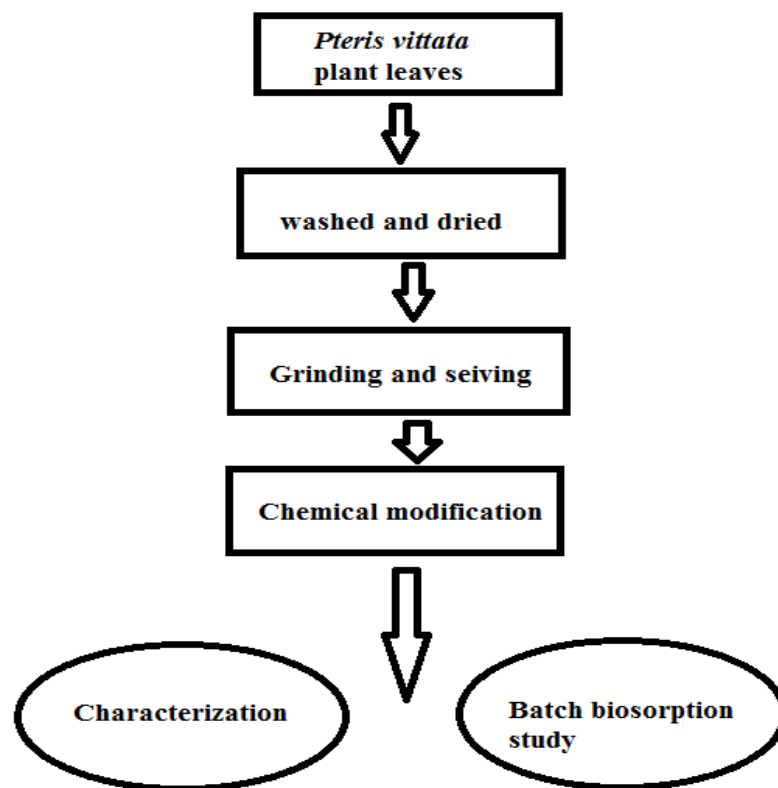


Figure 1. Protocol of CMPVL preparation.

2.3. Characterization of Biosorbent

To visualize the surface functionality, Fourier-transform infrared spectroscopy (PerkinElmer, Waltham, MA, USA) was used where the CMPVL spectra were recorded in the range of 400–4000 cm^{-1} for metal loaded and unloaded sample. A surface area analyzer was used to study the Brunauer–Emmett–Teller (BET) surface area and pore volume. Scanning electron microscopic analysis was conducted to see the morphological structure of both the loaded and unloaded samples of CMPVL. The thermo-gravimetric analysis (TGA) was conducted to check the stability of adsorbent. The elemental composition of the metal loaded and unloaded samples were evaluated by EDX (INCA200/Oxford Instruments, Abingdon, UK) analysis.

2.4. Batch Adsorption Experiment

For the adsorption tests, a stock solution of Cr(VI) in 1 L of distilled water was made and solutions of 20–300 mg/L (working dilutions) were subsequently obtained by diluting the stock solution. As chromium source $\text{K}_2\text{Cr}_2\text{O}_7$ (Sigma-Aldrich, Germany) have been used. In batch tests 50 mL of solution of each dilution were taken and added with 0.12 g of biomass then the mixture was shaken at a speed of 130 rpm for 120 min. After filtration, the amount of Cr(VI) was estimated using atomic absorption spectrophotometer with the help of equations given:

$$q_e = (C_i - C_f) \times \frac{V}{m} \quad (1)$$

$$\% R = \frac{(C_i - C_f)}{C_i} \times 100 \quad (2)$$

where C_i shows initial Cr(VI) concentration and C_f shows final concentration after adsorption. The V is the volume taken in liter for the batch test and m is the mass in g of adsorbent.

The other parameters are: V = volume, m = mass of sorbent, q_e = amount of metal adsorbed, whereas %R is percent removal of metal. Schematically, the batch adsorption experiments have been shown in Figure 2.

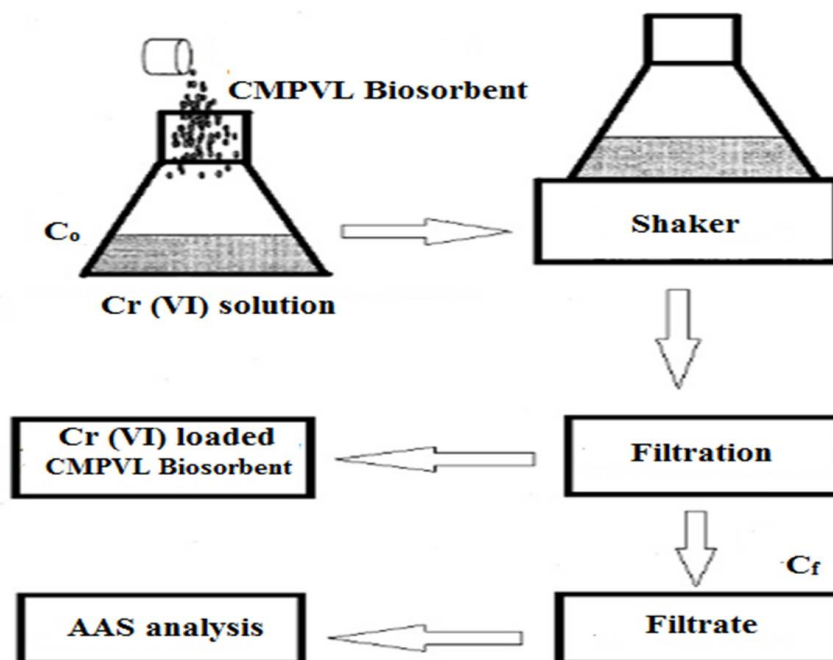


Figure 2. Scheme of batch biosorption experiment.

Different isotherm models such as Langmuir, Freundlich, Temkin, Harkin–Jura and Jovanovic were employed to evaluate the sorption parameters of prepared biosorbent.

2.5. Effect of Operating Physicochemical Parameters on the Sorption Process

In addition to isothermal studies, the effect of parameters such as biosorbent mass, pH of the solution, contact time, and temperature were also evaluated, where in each case, 50 mL metal solutions were contacted with a given quantity of sorbent, with the only changes in parameter under study. In the case of pH effect evaluation study, the solution pH was adjusted using NaOH (0.1 M) and HNO₃ (0.1 M), whereas in thermodynamics effect study the experiment were conducted at 293 K, 303 K, 313 K, 323 K and 333 K.

2.6. Kinetic Study

To investigate the kinetic characteristics of Cr(VI) biosorption on CMPVL, a set quantity of absorbent (0.12 g) was introduced into a series of flasks containing 50 mL of Cr(VI) solution (100 mg/L) which were then shaken at 130 rpm for different interval of time. The adsorption data obtained was fed into pseudo-first-order, pseudo-second-order, intra-particle diffusion model, Natarajan–Khalaf model and power function model to obtain an insight into kinetics of the process.

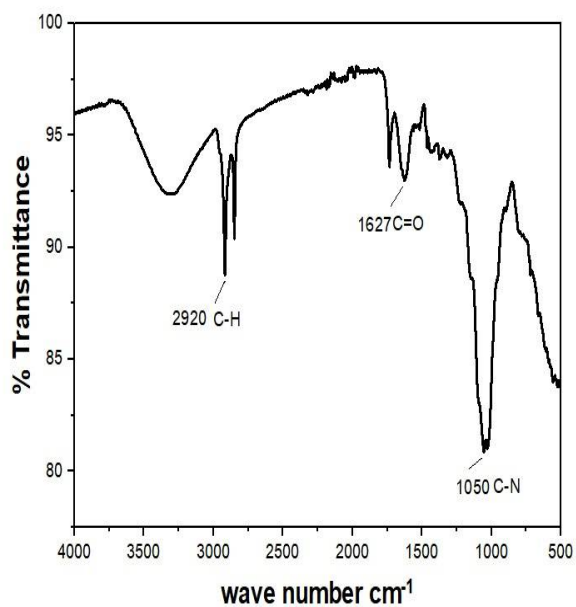
3. Result and Discussion

3.1. Characterization of CMPVL

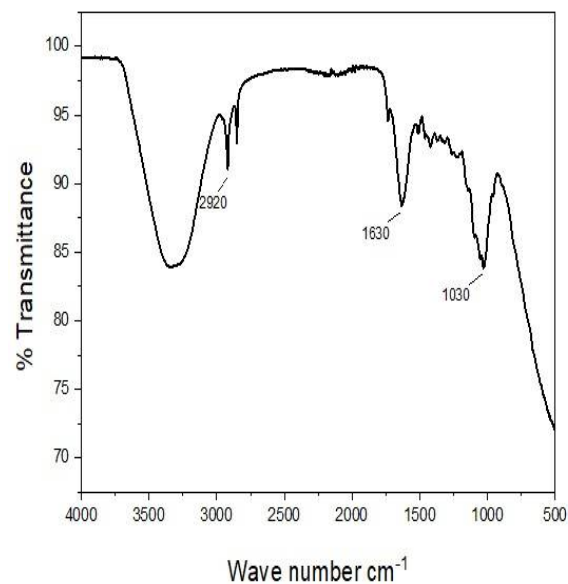
3.1.1. FTIR Spectra of Unloaded and Loaded Cr (VI) CMPVL

FTIR spectroscopy was utilized to examine the functional group in the unloaded biosorbent and the interaction between functional group of loaded biosorbent and metal ions. The unloaded and loaded spectra of CMPVL have been displayed in Figure 3A,B. The NH₂ group was deduced from the peak at 3200 cm⁻¹ to 3400 cm⁻¹, and the peak at 3000 to 3100 cm⁻¹ indicates the C-H stretch. The peak displayed between 1630–1680 cm⁻¹ is because of carbonyl group stretching and at 600 cm⁻¹ due to N-H group stretching.

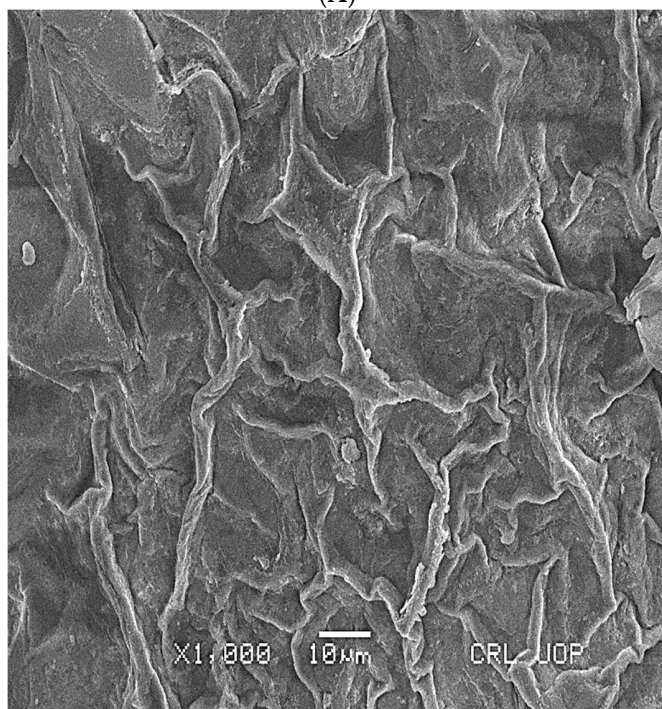
The spectra at $1100\text{--}1300\text{ cm}^{-1}$ show the C-N group stretching [20]. The loaded spectra Figure 3B of CMPVL represents that at 3300 cm^{-1} O-H stretching and at 2930 cm^{-1} C-H stretch was reported. The peak at 1630 is for C=C stretching and at 1030 cm^{-1} for C-O stretch. A slight shift in the peak of loaded adsorbent has been reported.



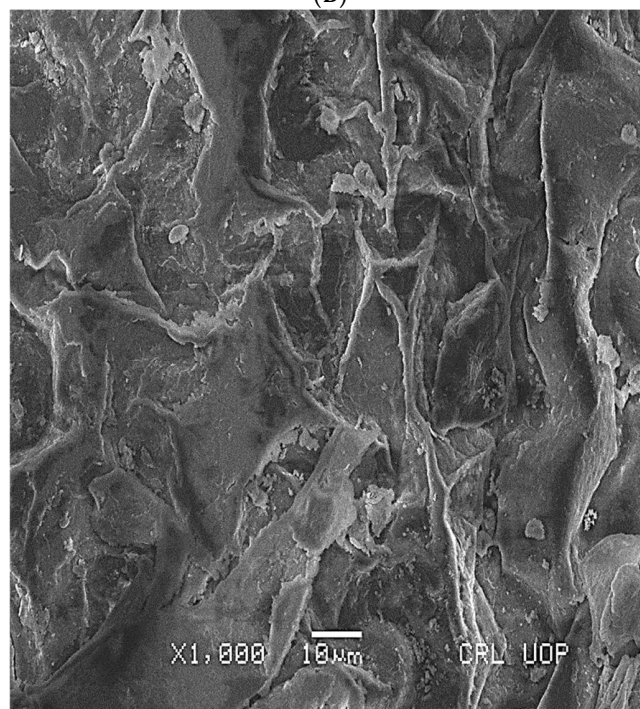
(A)



(B)



(C)



(D)

Figure 3. Cont.

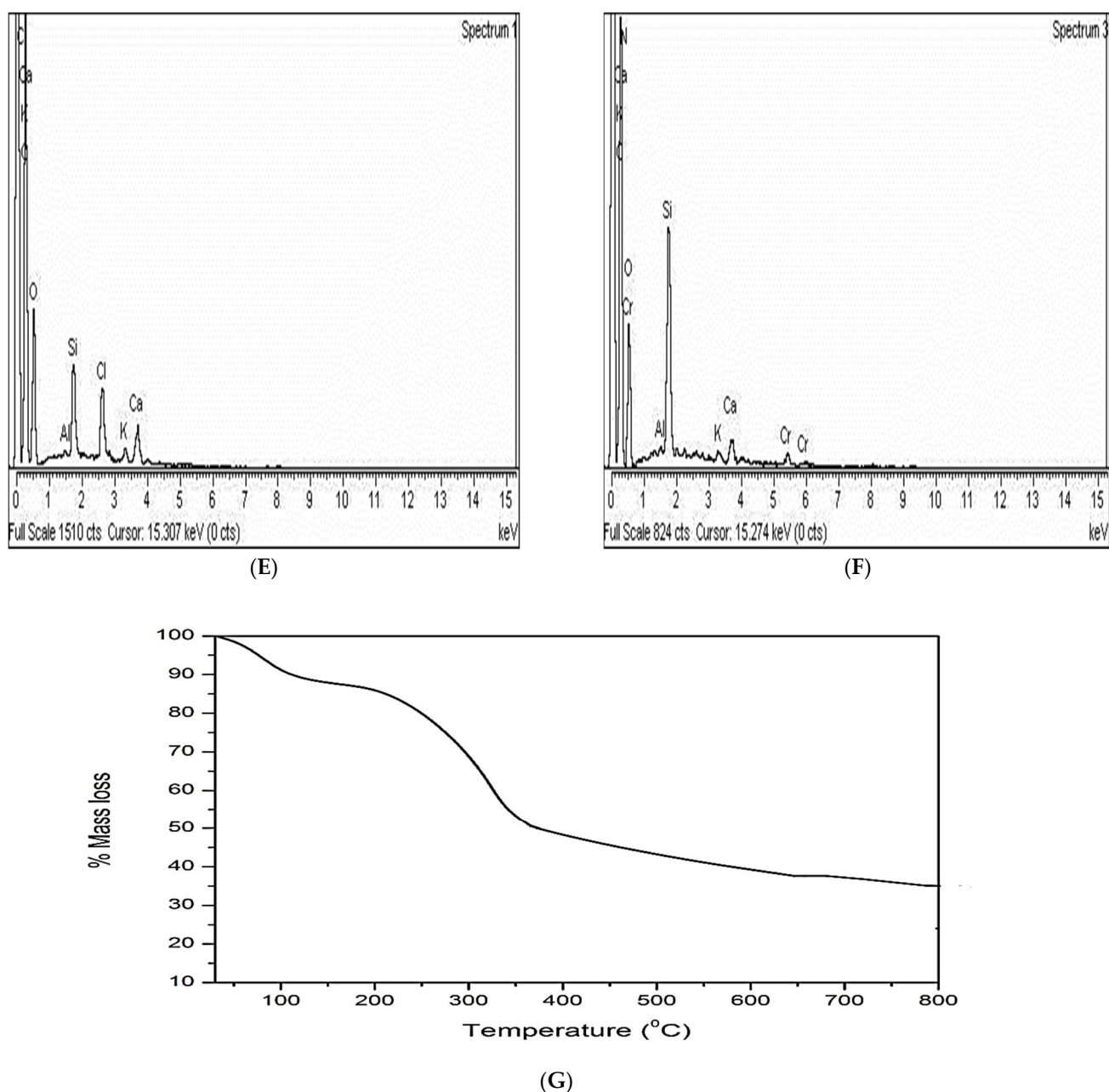


Figure 3. (A) Unloaded CMPVL FTIR Spectrum; (B) loaded CMPVL FTIR Spectrum; (C) SEM image of CMPVL; (D) SEM image of Cr(VI)-loaded CMPVL; (E) EDX plot for CMPVL; (F) EDX plot for Cr(VI)-loaded CMPVL; (G) TGA plot for CMPVL.

3.1.2. Surface Area and Pore Volume

The BET surface area and pore volume of CMPVL are all presented in Table 1. According to this, CMPVL has a larger surface area and greater pores, making it a good biosorbent in terms of biosorption capacity [20].

Table 1. Surface area, pore volume and diameter of CMPVL.

Biosorbent	CMPVL
BET surface area (m ² /g)	73.28
Pore volume (cc/g)	0.82

3.1.3. SEM Analysis

SEM images of treated and Cr-loaded biosorbent are displayed in Figure 3C,D, which illustrate the surface morphology and roughness of treated biosorbent. The pictures display a clear, porous structure with curves and bent edges that could be an appropriate surface for adsorption. The SEM images of loaded adsorbent showed that the surface was occupied by Cr(VI).

3.1.4. EDX Analysis

The elemental analysis of unloaded and Cr (VI)-loaded biosorbent is displayed in Figure 3E,F. In comparison with other tiny peaks of Ca, Si, K, S, P, Cl, and Mg that appeared as impurities, the oxygen and carbon peaks are more prominent in the unloaded biosorbent. The loaded biosorbent displayed an apparent peak of Cr, which represents the biosorption of Cr(VI) on CMPVL.

3.1.5. Thermal Gravimetric Analysis

The TGA analysis is displayed in Figure 3G. The sample of treated biosorbent examined for the thermal gravimetric investigation was 7.873 mg. The mass loss occurred with respect to temperature in three stages. In the first stage, the mass loss occurred with respect to temperature due to water evaporation, followed by the second stage, which was because of the breakdown of cellulose. In the third stage, the mass loss occurred due to the formation of carbonaceous material, and after that, stability of the sample was seen at round 800 °C.

3.2. Adsorption Isothermal Studies

Up to a certain point, the amount of metal removed by the adsorbent rises with an increase in starting concentration; after that, no further increase is reported in adsorption capacity as the adsorbent has reached the point of its saturation and the pores available for the adsorption were fully occupied [21]. Figure 4A shows that when the starting concentration of Cr(VI) was raised, a high speed in the biosorption process were reported until the biosorbent pores were fully occupied by Cr(VI) metal ion, and after that, a decline in the biosorption process was noticed. A number of isothermal models such as Freundlich, Langmuir, Temkin, Harkins–Jura and Jovanovic isotherm were utilized to describe the parameters of adsorption.

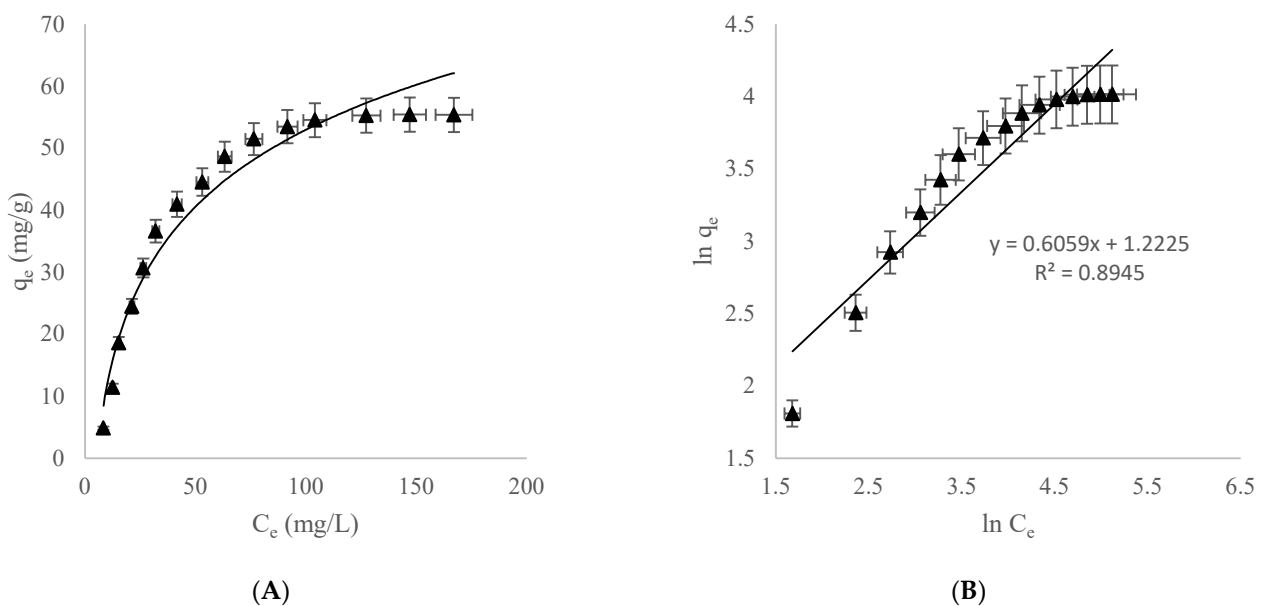
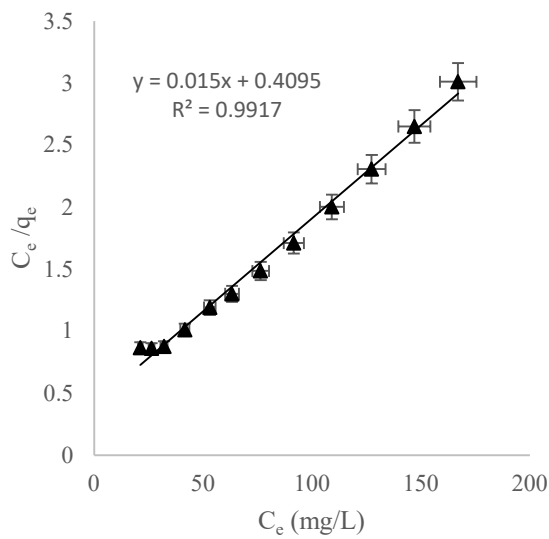
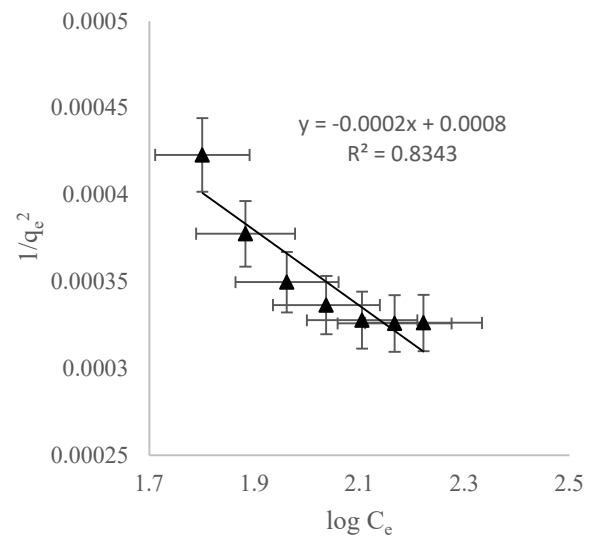


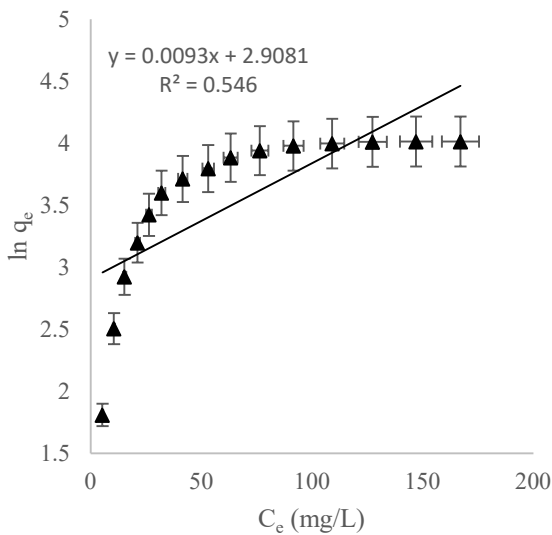
Figure 4. Cont.



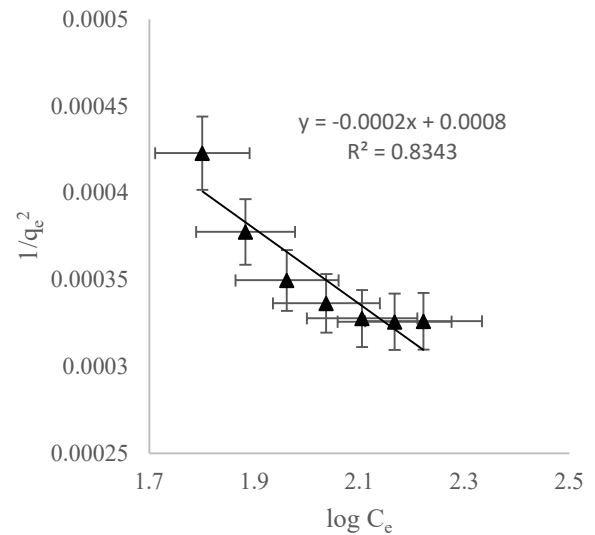
(C)



(D)



(E)



(F)

Figure 4. Adsorption isothermal study. (A) Effect of initial Cr(VI) concentration; (B) Langmuir adsorption isotherm; (C) Freundlich adsorption isotherm; (D) Temkin adsorption isotherm; (E) Jovanovic adsorption isotherm; (F) Harkins–Jura adsorption isotherm.

3.2.1. Freundlich Adsorption Isotherm

The adsorption is multilayer with binding sites possessing various energies are described by this model [22]. This model’s mathematical expression can be as given:

$$\ln q_e = \log K_F + \frac{1}{n} \ln C_e \tag{3}$$

where the equilibrium concentrations represented by C_e in the solution and q_e (mg/g) is the quantity of Cr(VI) adsorbed per unit mass of CMPVL. The slope and intercept of the $\ln q_e$ vs. C_e plot, displayed in Figure 4B, can be used to calculate the Freundlich constant (K_F) and the adsorption coefficient (n), whose values are listed in Table 2.

Table 2. Isothermal parameters for adsorption of Cr (VI) on CMPVL.

Adsorption Isotherm	Parameters	Values
Langmuir	q_{\max} (mg/g)	66.6
	K_L (L/mg)	0.03671
	R^2	0.991
Freundlich	K_F (mg/g)	3.394
	n	1.653
	R^2	0.894
Temkin	β	16.57
	α	4.197
	b	136.98
	R^2	0.968
Jovanovich	K_J (L/g)	0.009
	q_{\max} (mg/g)	18.32
	R^2	0.546
Harkins–Jura	A_H (g ² /L)	5
	B_H (mg ² /L)	4
	R^2	0.834

3.2.2. Langmuir Adsorption Isotherm

This model can be expressed in the following linear form [23].

$$\frac{C_e}{q_e} = \frac{1}{q_{m \times b}} + \frac{C_e}{q_m} \quad (4)$$

The maximum adsorption capacity is indicated by q_m while the C_e and q_e as aforementioned. The Langmuir constant, which is concerned with free energy as well as binding strength, is referred as “ b ”. When C_e vs. C_e/q_e were plotted, Figure 4C shows a linear curve with b and q_{\max} as the intercept and slope, respectively. Higher R^2 (0.991) value indicates that experimental data can be well managed by the model. Thus the parameters of this model were calculated and expressed in Table 2.

3.2.3. Temkin Adsorption Isotherm

Adsorption heat and surface coverage are related by Temkin adsorption isotherm. The mathematical form of this model is given below [24,25].

$$q_e = \beta \ln \alpha + \beta \ln C_e \quad (5)$$

where $\beta = RT/b$, R has a value of 8.314 J/mol K, and is called ideal gas constant, b represents a constant which is related to the heat of adsorption and T indicates the absolute temperature. The plot drawn between q_e vs. $\ln C_e$ is displayed in Figure 4D and the β , b and R^2 values calculated from the graph were listed in Table 2.

3.2.4. Jovanovic Adsorption Isotherm

The mechanical link between adsorbent and adsorbate is described by this model. The mathematical form of the isotherm can be expressed in the given form [26].

$$\ln q_e = \ln q_{\max} - K_J C_e \quad (6)$$

C_e and q_{\max} can be inferred from the graph intercept. The slope and intercept of the $\ln q_e$ vs. C_e plot, as seen in Figure 4E, were used to calculate the K_J and q_{\max} values that are enlisted in Table 2.

3.2.5. Harkins—Jura Adsorption Isotherm

This model reflects the probability of multilayer adsorption on an adsorbent surface having a different porous arrangement [27].

$$\frac{1}{q_e^2} = \frac{B_H}{A_H} - \frac{1}{A_H} \log C_e \tag{7}$$

The intercept and slope of the graph depicted in Figure 4F were used to compute the B_H and A_H constants, and their values are given in Table 2.

3.3. Impact of Contact Time and Kinetic Study

Figure 5A shows the impact of contact time on the biosorption of Cr (VI) on CMPVL. The increased accessibility of empty holes for the adsorbate is the cause of the increased adsorption of Cr (VI) on CMPVL with a time up to 20 min. Following the rapid stage, the biosorption process gradually slows down, representing a consistent rate of sorption, which eventually caused the saturation of binding sites. After 120 min, equilibrium was reached. The kinetic parameters of Cr (VI) biosorption on CMPVL could be calculated by applying the pseudo-first-order model, pseudo-second-order model, Natarajan–Khalaf models, intraparticle and power function to the experimental kinetic data.

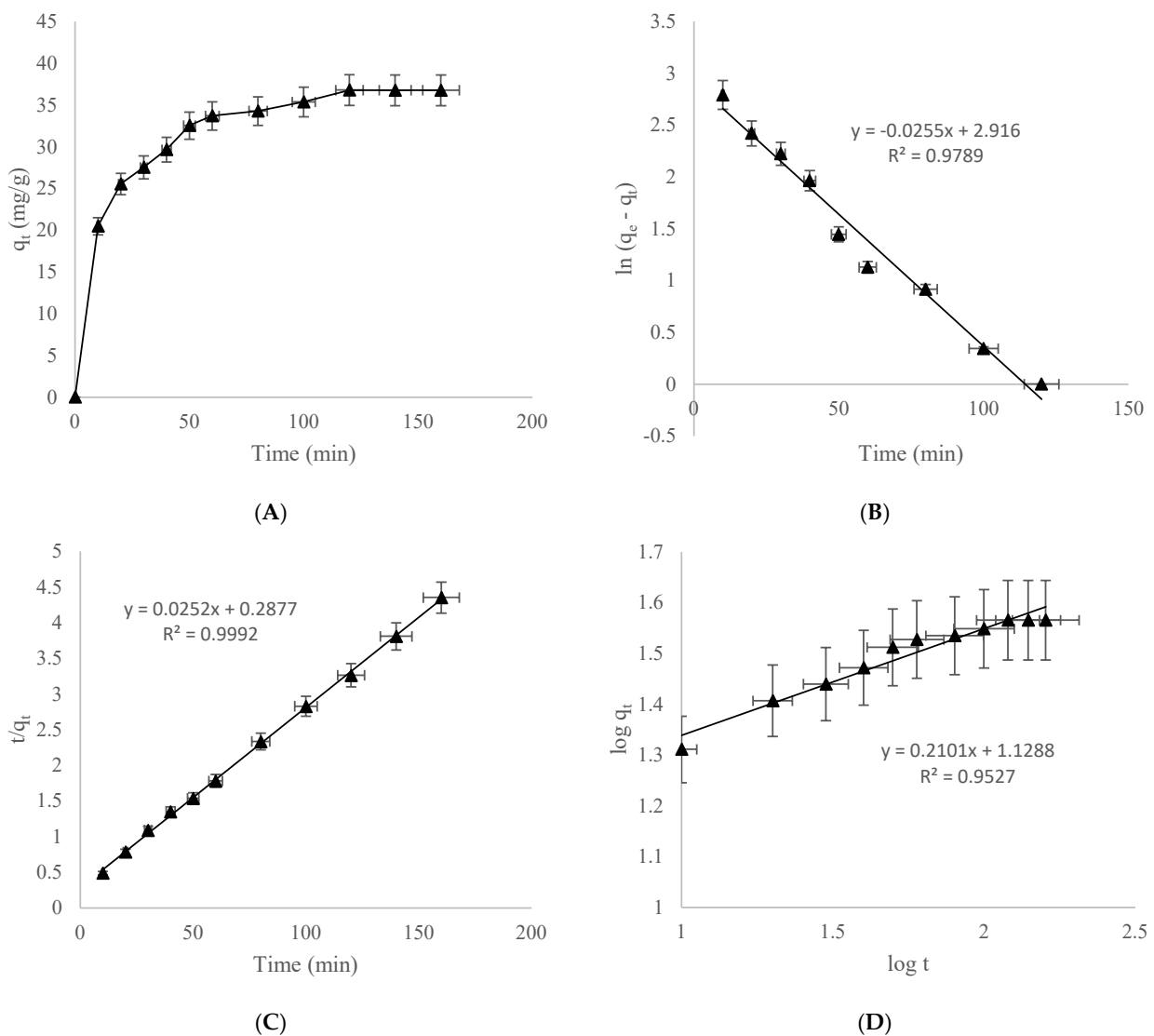


Figure 5. Cont.

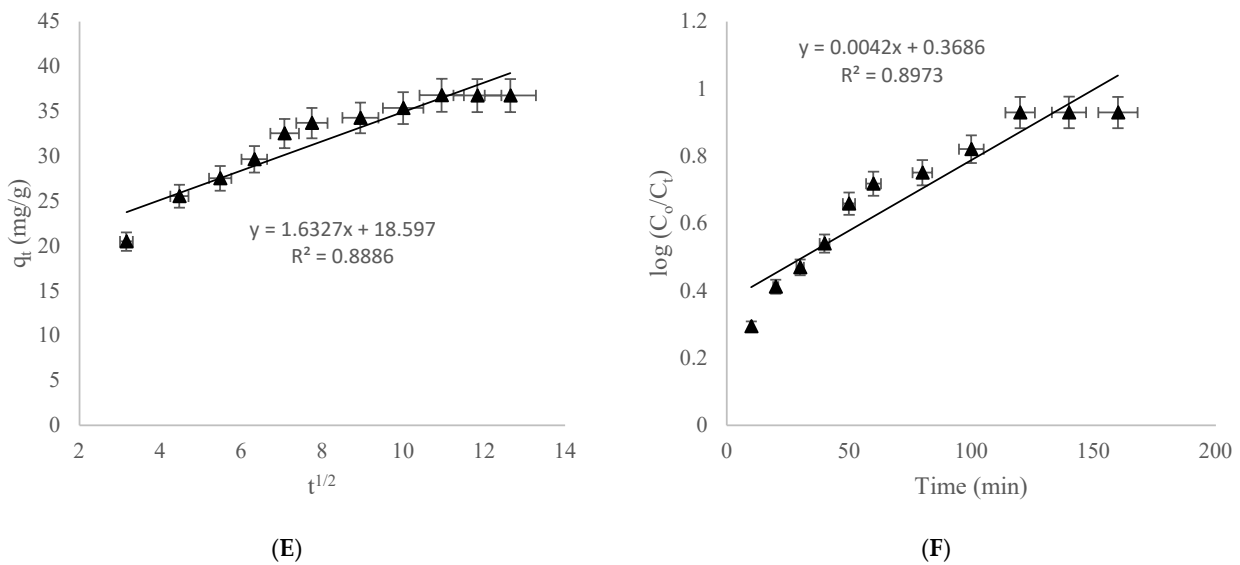


Figure 5. (A) Impact of contact time; (B) pseudo-first-order kinetic model; (C) pseudo-second-order kinetic model; (D) power function kinetic model; (E) intraparticle kinetic model; (F) Natarajan–Khalaf kinetic model.

3.3.1. Pseudo-First-Order Kinetic Model

The mathematical form of this model is given below [28].

$$\ln(q_e - q_t) = \ln q_e - K_1 t \tag{8}$$

The q_e (mg/g) and q_t (mg/g) represent the amounts of metal adsorbed at equilibrium and at time t , while K_1 is the rate constant. Table 3 displays the values of K_1 and q_e as computed from the slope and intercept of the $\ln(q_e - q_t)$ vs. t plot, as displayed in Figure 5B. The values of kinetics constants are given in Table 3.

Table 3. Kinetic parameters for Cr (VI) biosorption on CMPVL.

Kinetic Model	Parameters	Values
Pseudo-first-order	K_1 (1/min)	−0.025
	q_e (mg/g)	18.467
	R^2	0.978
Pseudo-second-order	K_2 (1/min)	0.287
	q_e (mg/g)	40
	R^2	0.999
Power function	α	13.427
	b	0.210
	R^2	0.952
Intra particle diffusion	K_{diff} (mg/g min ^{1/2})	1.632
	C	18.59
	R^2	0.888
Natarajan–Khalaf	K_N (1/min)	9.2×10^{-3}
	R^2	0.897

3.3.2. Pseudo-Second-Order Kinetic Model

Following is the mathematical form of the model [29].

$$t/q_t = 1/K_2 q_e^2 + t/q_e \tag{9}$$

All other parameters in equation are specified above, except K_2 that is a pseudo-second-order constant, which was determined from the intercept of the plot, as shown in Figure 5C and as enlisted in Table 3.

3.3.3. Power Function Kinetic Model

Following is the linear form of this model [30].

$$\log q_t = \log a + b \log t \quad (10)$$

In this equation, constants a and b represent the initial rate of adsorption and the reaction rate, respectively. Their values could be computed using the intercept and slope of the $\log q_t$ vs. $\log t$ plot, as given in Figure 5D, and Table 3 displayed their values.

3.3.4. Intraparticle Kinetic Model

The representation of this model is described below [31,32].

$$q_t = K_{\text{diff}} t^{1/2} + C \quad (11)$$

where K_{diff} ($\text{mg g}^{-1} \text{min}^{1/2}$) is the rate constant for this model. The intercept of the q_t vs. $t^{1/2}$ graph can be used to calculate the constant C (mg g^{-1}), which is related to the boundary layer's thickness. Table 3 provides a list of their values. The intraparticle diffusion curve was produced by plotting q_t vs. $t^{1/2}$ is shown in Figure 5E.

3.3.5. Natarajan–Khalaf Kinetic Model

Following is the mathematical form of this model [33].

$$\log \left(\frac{C_0}{C_t} \right) = \frac{K_N}{2.303} t \quad (12)$$

According to this equation, C_0 (mg/L) and C_t (mg/L) stands for the initial and final concentration at time t , respectively, and K_N (mg/L) for a constant that can be measured from the slope of graph, as shown in Figure 5F.

3.4. pH Analysis

The effect of pH on Cr (VI) biosorption was investigated in the pH ranging 2–7, as shown in Figure 6. The various dissociation states of Cr should be distributed differentially in aqueous solution depending on pH. Chromium exists in the form of $\text{Cr}_2\text{O}_7^{-2}$, HCrO_4^- and CrO_4^{-2} in aqueous solution depending on pH. In the acidic pH range, Cr exists in the $\text{Cr}_2\text{O}_7^{-2}$ and HCrO_4^- , and above pH 7, the stable species is CrO_4^{-2} . The maximal removal of Cr(VI) was reported at pH 2, while at high Ph, the uptake capacities were decreased. At pH = 2, the adsorbent's surface become positively charged and HCrO_4^- is the main form which exists at this pH. Thus, at low pH, the attraction between adsorbent and the anion of Cr results in increased adsorption of Cr (VI). However, at pH = 5 or higher, the HCrO_4^- anions of Cr(VI) changes into CrO_4^{-2} form and so the competition between these species and OH^- result in the decline of Cr(VI) adsorption [34,35]. It was reported that at lower pH, the system attains equilibrium faster, and also, the percentage of chromium adsorption was increased. Therefore, the optimum pH = 2 was obtained for the batch adsorption tests.

3.5. Biosorbent Dose Effect

The impact of biosorbent dose (0.01–0.13 g) on the elimination of Cr(VI) was analyzed in the batch adsorption tests. Figure 7 displays the relation between the adsorbent dose and Cr(VI) removal. The elimination of Cr(VI) was enhanced by increasing biosorbent dose from 0.01 to 0.12 g. The highest elimination of Cr(VI) at higher biosorbent dose (0.12 g) was because of the risen surface area and presence of more active sites which made it possible [36,37]. Therefore, the optimum dose of 0.12 g was taken for the batch tests.

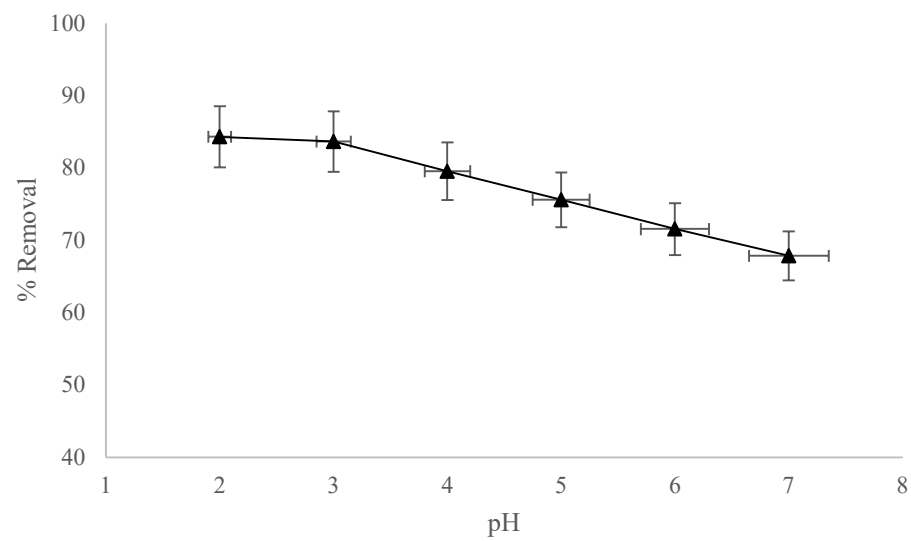


Figure 6. Effect of pH on Cr (VI) biosorption by CMPVL.

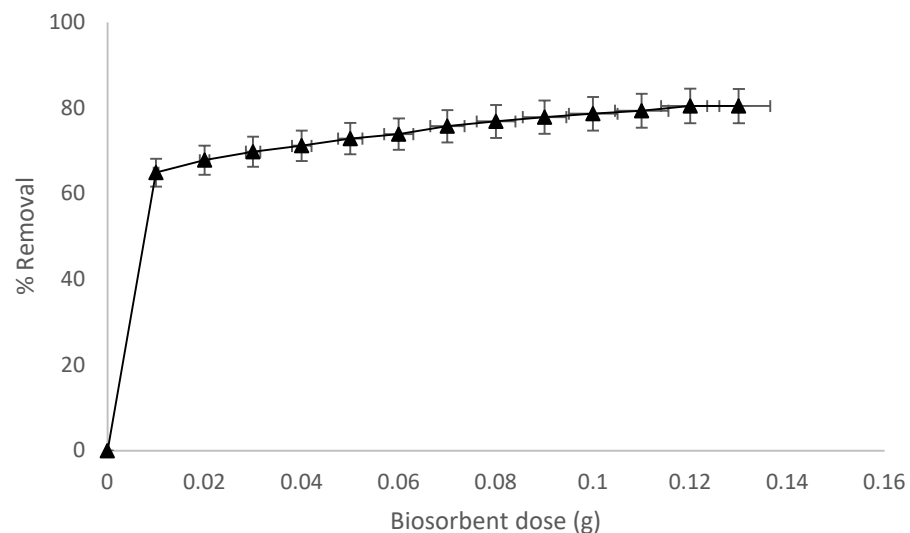


Figure 7. Impact of biosorbent dose.

3.6. Adsorption Thermodynamics

The study of thermodynamics is crucial, and it determines the nature and the effectiveness of the given biosorption process. By knowing the nature of the biosorption process, namely, whether it is exothermic or endothermic, is crucial from the industrial perspective. The batch adsorption experiments were carried out at different temperatures (293, 303, 313, 323, 333 K) to find out the thermodynamic parameters. The mechanism driving the increase in adsorption with temperature could be the low kinetic energy of $\text{Cr}_2\text{O}_7^{-2}$ at lower temperature and the insufficient interaction between $\text{Cr}_2\text{O}_7^{-2}$ and the active site. The kinetic energy increases with increasing temperature, which result in the maximum binding capacity. By using Van 't Hoff plot (Figure 8) the enthalpy change (ΔH°) and entropy change (ΔS°) were computed, and their values were listed in Table 4. The positive value of ΔS° and negative value of ΔH° displayed that these processes were spontaneous and exothermic. Following is the presentation of the Van 't Hoff equation [38]:

$$\ln K = \frac{\Delta S^\circ}{R} - \frac{\Delta H^\circ}{RT} \quad (13)$$

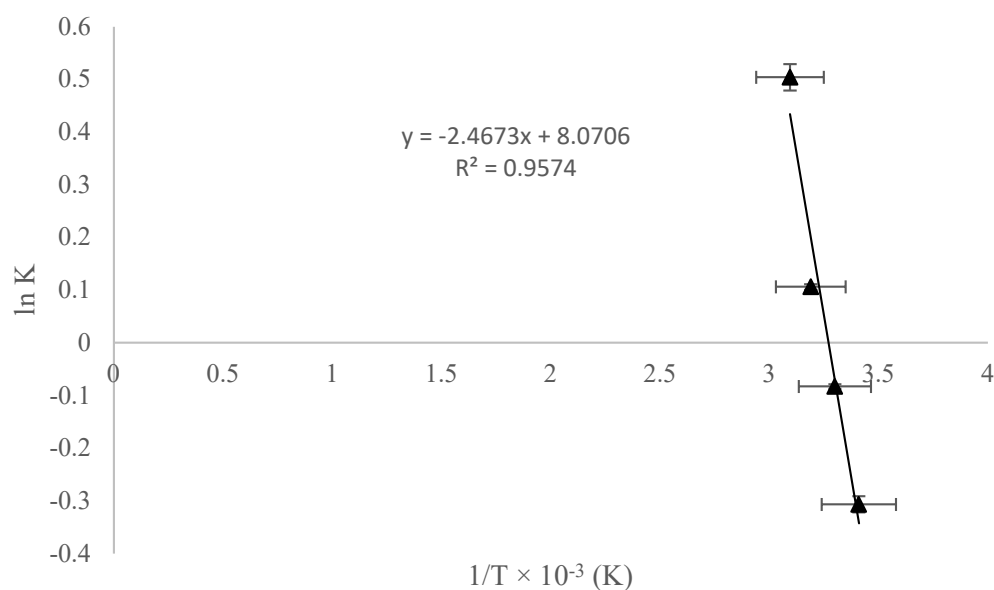


Figure 8. Thermodynamic study of Cr(VI) adsorption by CMPVL.

Table 4. Thermodynamic parameters for Cr (VI) biosorption on CMPVL.

Parameters	Values	Values
ΔH° (J/mol K)		-20.51
ΔS° (J/mol K)		67.09
	ΔG° (KJ/mol)	
293 K		-19.67
303 K		-20.34
313 K		-21.019
323 K		-21.69
333 K		-22.36

In the above equation q_e (mg/g), C_e , R and T are as stated above. The following equation was used to compute Gibbs energy change ΔG° [39].

$$\Delta G^\circ = \Delta H^\circ - T\Delta S^\circ \quad (14)$$

The values of ΔG° were shown in Table 3, which shows the spontaneous and favorable aspect of the biosorption process.

3.7. Regeneration of CMPVL Biosorbent

The CMPVL biosorbent was regenerated and reused for five cycles, where the fall in Cr (VI) removal efficiency was 27%, which indicates that regenerated CMPVL biosorbent could be efficiently reused repeatedly. Figure 9 shows the decline in % removal of Cr(VI) with an increase in regeneration.

3.8. Comparison of Adsorption Capacities of CMPVL with the Literature

A comparison of CMPVL with reported adsorbent capacities has been shown in Table 5. The adsorption capacities of CMPVL are reasonably high as compared to the one cited in the table.

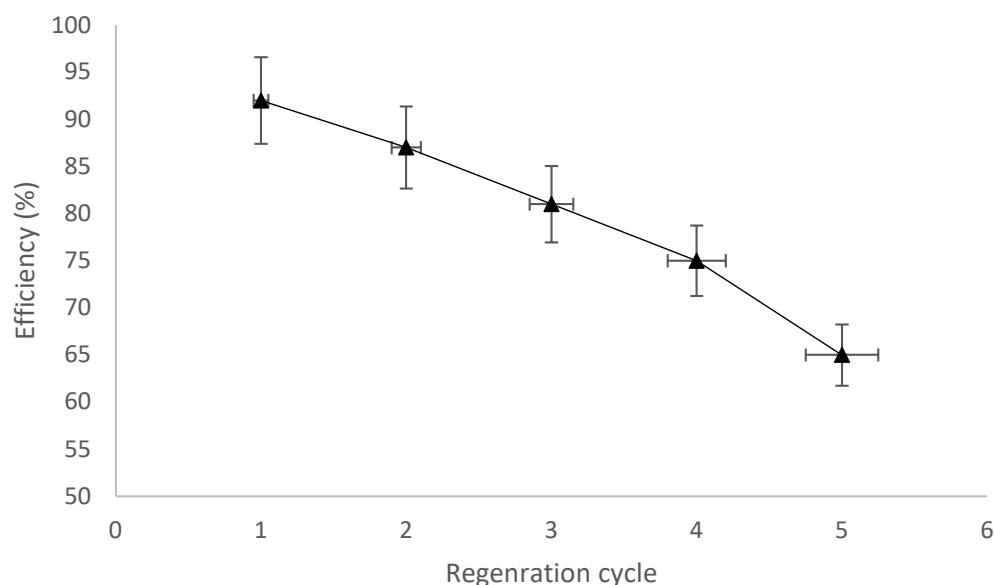


Figure 9. Decrease in percent efficiency of Cr(VI) removal for 5 consecutive cycle.

Table 5. Biosorption capacity comparison of CMPVL with the literature.

S.NO	Biosorbent	q_{\max} (mgg ⁻¹)	References
1	This research work	66.67	
2	<i>Melaleuca diosmifolia</i> leaf	62.5	[40]
3	CMSML	93.45	[41]
4	Carbonized pineapple leaves	18.77	[42]
5	<i>Magnolia</i> leaf biomass	12.3	[43]
6	chemically modified <i>Polyalthia longifolia</i> leaves	5.128	[44]

4. Conclusions

In this study, the intrinsic affinity of a plant, the phytoremediation capacity was utilized in designing an efficient adsorbent. The CMPVL a low-cost and environmentally friendly adsorbent was used to reduce Cr(VI) concentration in the industrial effluents. The effect of initial pH, contact time, biosorbent dose, initial metal concentration, and temperature on adsorption process were evaluated in order to optimize the sorption process. The optimum parameters recorded were pH = 2, biosorbent dose = 0.12 g, contact period = 120 min, initial Cr(VI) concentration = 100 mg/L, and temperature = 30 °C. Langmuir isotherm with an R^2 value of 0.991 was found to be the most suitable isotherm model among tested ones. According to a kinetic investigation of Cr (VI) the biosorption follow pseudo-second-order kinetics pointing towards the chemical nature of the process. From values and signs of the thermodynamic parameters estimated, it was inferred that the sorption process investigated herein is favorable, spontaneous, and exothermic. FTIR, SEM, EDX and TGA analysis were also performed to explain the chemical and physical basis of the sorption process. In a nutshell, we conclude that the elimination of Cr(VI) from water might be accomplished successfully in an environmentally friendly way through CMPVL.

Author Contributions: Conceptualization, M.Z.; Paper write up and review, M.Z., Q.K. and M.W.; Supervision, S.M.S. and M.Z.; Formal analysis, A.W.K. and M.T. All authors have read and agreed to the published version of the manuscript.

Funding: No external funding has been received.

Institutional Review Board Statement: Not applicable.

Informed Consent Statement: Not applicable.

Conflicts of Interest: The authors declare no conflict of interest.

References

1. Jeyaseelan, C.; Gupta, A. Green tea leaves as a natural adsorbent for the removal of Cr (VI) from aqueous solutions. *Air Soil Water Res.* **2016**, *9*, ASWR-S35227. [[CrossRef](#)]
2. Shirzad, S.M.; Samarghandi, M.; Azizian, S.; Kim, W.; Lee, S. The removal of hexavalent chromium from aqueous solutions using modified holly sawdust: Equilibrium and kinetics studies. *Environ. Eng. Res.* **2011**, *16*, 55–60.
3. Zhou, J.; Wu, P.; Dang, Z.; Zhu, N.; Li, P.; Wu, J.; Wang, X. Polymeric Fe/Zr pillared montmorillonite for the removal of Cr (VI) from aqueous solutions. *Chem. Eng. J.* **2010**, *162*, 1035–1044. [[CrossRef](#)]
4. Yasuda, M.; Miwa, A.; Kitagawa, M. Morphometric studies of renal lesions in itai-itai disease: Chronic cadmium nephropathy. *Nephron* **1995**, *69*, 14–19. [[CrossRef](#)]
5. Kadirvelu, K.; Thamaraiselvi, K.; Namasivayam, C. Removal of heavy metals from industrial wastewaters by adsorption onto activated carbon prepared from an agricultural solid waste. *Bioresour. Technol.* **2001**, *76*, 63–65. [[CrossRef](#)]
6. Wilbur, S.; Abadin, H.; Fay, M.; Yu, D.; Tencza, B.; Ingerman, L.; Klotzbach, J.; James, S. *Toxicological Profile for Chromium*; Agency for Toxic Substances and Disease Registry (US): Atlanta, GA, USA, 2012. [[PubMed](#)]
7. Akram, M.; Bhatti, H.N.; Iqbal, M.; Noreen, S.; Sadaf, S. Biocomposite efficiency for Cr (VI) adsorption: Kinetic, equilibrium and thermodynamics studies. *J. Environ. Chem. Eng.* **2017**, *5*, 400–411. [[CrossRef](#)]
8. Zheng, C.; Zheng, H.; Wang, Y.; Wang, Y.; Qu, W.; An, Q.; Liu, Y. Synthesis of novel modified magnetic chitosan particles and their adsorption performance toward Cr (VI). *Bioresour. Technol.* **2018**, *267*, 1–8. [[CrossRef](#)]
9. Ye, Z.; Yin, X.; Chen, L.; He, X.; Lin, Z.; Liu, C.; Ning, S.; Wang, X.; Wei, Y. An integrated process for removal and recovery of Cr (VI) from electroplating wastewater by ion exchange and reduction–precipitation based on a silica-supported pyridine resin. *J. Clean. Prod.* **2019**, *236*, 117631. [[CrossRef](#)]
10. Yang, X.; Liu, L.; Zhang, M.; Tan, W.; Qiu, G.; Zheng, L. Improved removal capacity of magnetite for Cr (VI) by electrochemical reduction. *J. Hazard. Mater.* **2019**, *374*, 26–34. [[CrossRef](#)]
11. Kretschmer, I.; Senn, A.M.; Meichtry, J.M.; Custo, G.; Halac, E.B.; Dillert, R.; Bahnemann, D.W.; Litter, M.I. Photocatalytic reduction of Cr (VI) on hematite nanoparticles in the presence of oxalate and citrate. *Appl. Catal. B Environ.* **2019**, *242*, 218–226. [[CrossRef](#)]
12. Jin, W.; Du, H.; Zheng, S.; Zhang, Y. Electrochemical processes for the environmental remediation of toxic Cr (VI): A review. *Electrochim. Acta* **2016**, *191*, 1044–1055. [[CrossRef](#)]
13. Muthusaravanan, S.; Sivarajasekar, N.; Vivek, J.; Paramasivan, T.; Naushad, M.; Prakashmaran, J.; Gayathri, V.; Al-Duaij, O.K. Phytoremediation of heavy metals: Mechanisms, methods and enhancements. *Environ. Chem. Lett.* **2018**, *16*, 1339–1359. [[CrossRef](#)]
14. Kausar, A.; MacKinnon, G.; Alharthi, A.; Hargreaves, J.; Bhatti, H.N.; Iqbal, M. A green approach for the removal of Sr (II) from aqueous media: Kinetics, isotherms and thermodynamic studies. *J. Mol. Liq.* **2018**, *257*, 164–172. [[CrossRef](#)]
15. Kausar, A.; Bhatti, H.N.; Iqbal, M.; Ashraf, A. Batch versus column modes for the adsorption of radioactive metal onto rice husk waste: Conditions optimization through response surface methodology. *Water Sci. Technol.* **2017**, *76*, 1035–1043. [[CrossRef](#)]
16. Azzaz, A.A.; Jellali, S.; Assadi, A.A.; Bousselmi, L. Chemical treatment of orange tree sawdust for a cationic dye enhancement removal from aqueous solutions: Kinetic, equilibrium and thermodynamic studies. *Desalination Water Treat.* **2016**, *57*, 22107–22119. [[CrossRef](#)]
17. Azzaz, A.A.; Jellali, S.; Akrouf, H.; Assadi, A.A.; Bousselmi, L. Optimization of a cationic dye removal by a chemically modified agriculture by-product using response surface methodology: Biomasses characterization and adsorption properties. *Environ. Sci. Pollut. Res.* **2017**, *24*, 9831–9846. [[CrossRef](#)]
18. La, D.D.; Nguyen-Tri, P.; Le, K.H.; Nguyen, P.T.; Nguyen, M.D.B.; Vo, A.T.; Nguyen, D.D. Effects of antibacterial ZnO nanoparticles on the performance of a chitosan/gum arabic edible coating for post-harvest banana preservation. *Prog. Org. Coat.* **2021**, *151*, 106057. [[CrossRef](#)]
19. Zhu, S.; Xia, M.; Chu, Y.; Khan, M.A.; Lei, W.; Wang, F.; Wang, A. Adsorption and desorption of Pb (II) on l-lysine modified montmorillonite and the simulation of interlayer structure. *Appl. Clay Sci.* **2019**, *169*, 40–47. [[CrossRef](#)]
20. Khan, Q.; Zahoor, M.; Salman, S.M.; Wahab, M.; Khan, F.A.; Gulfam, N.; Zekker, I. Removal of Iron (II) from Effluents of Steel Mills Using Chemically Modified Pteris vittata Plant Leaves Utilizing the Idea of Phytoremediation. *Water* **2022**, *14*, 2004. [[CrossRef](#)]
21. Langmuir, I. The adsorption of gases on plane surfaces of glass, mica and platinum. *J. Am. Chem. Soc.* **1918**, *40*, 1361–1403. [[CrossRef](#)]
22. Freundlich, H. Über die adsorption in lösungen. *Z. Für Phys. Chem.* **1907**, *57*, 385–470. [[CrossRef](#)]
23. Langmuir, I. The constitution and fundamental properties of solids and liquids. Part I. Solids. *J. Am. Chem. Soc.* **1916**, *38*, 2221–2295. [[CrossRef](#)]
24. Shahbeig, H.; Bagheri, N.; Ghorbanian, S.A.; Hallajisani, A.; Poorkarimi, S. A new adsorption isotherm model of aqueous solutions on granular activated carbon. *World J. Model. Simul.* **2013**, *9*, 243–254.
25. Samarghandi, M.; Hadi, M.; Moayedi, S.; BARJESTEHEH, A.F. Two-parameter isotherms of methyl orange sorption by pinecone derived activated carbon. *J. Environ. Health Sci. Eng.* **2009**, *6*, 285–294.

26. Foo, K.Y.; Hameed, B.H. Insights into the modeling of adsorption isotherm systems. *Chem. Eng. J.* **2010**, *156*, 2–10. [[CrossRef](#)]
27. Ramesh, S.; Rameshbabu, N.; Gandhimathi, R.; Srikanth Kumar, M.; Nidheesh, P. Adsorptive removal of Pb (II) from aqueous solution using nano-sized hydroxyapatite. *Appl. Water Sci.* **2013**, *3*, 105–113. [[CrossRef](#)]
28. McKay, G.; Ho, Y.; Ng, J. Biosorption of copper from waste waters: A review. *Sep. Purif. Methods* **1999**, *28*, 87–125. [[CrossRef](#)]
29. Simonin, J.-P. On the comparison of pseudo-first order and pseudo-second order rate laws in the modeling of adsorption kinetics. *Chem. Eng. J.* **2016**, *300*, 254–263. [[CrossRef](#)]
30. Terpinc, P.; Bezjak, M.; Abramovič, H. A kinetic model for evaluation of the antioxidant activity of several rosemary extracts. *Food Chem.* **2009**, *115*, 740–744. [[CrossRef](#)]
31. Srivastava, S.; Tyagi, R.; Pant, N. Adsorption of heavy metal ions on carbonaceous material developed from the waste slurry generated in local fertilizer plants. *Water Res.* **1989**, *23*, 1161–1165. [[CrossRef](#)]
32. Weber, W.J., Jr.; Morris, J.C. Kinetics of adsorption on carbon from solution. *J. Sanit. Eng. Div.* **1963**, *89*, 31–59. [[CrossRef](#)]
33. Ramulu, N.; Thirumurugan, V.; Krishnaveni, S.; Rajajeyaganthan, R. Adsorption of Rhodamine-B dye from an aqueous solution by biomass pine apple peel: Kinetics, equilibrium and thermodynamic studies. *SOJ Mater. Sci. Eng.* **2016**, *4*, 1–9.
34. Tiwari, D.; Promod, K.; Mishra, A.; Singh, R.; Srivastav, R. Removal of toxic metals from electroplating industries (effect of pH on removal by adsorption). *Indian J. Environ. Health* **1989**, *31*, 120–124.
35. Saravanane, R.; Sundararajan, T.; Reddy, S.S. Efficiency of chemically modified low cost adsorbents for the removal of heavy metals from waste water: A comparative study. *Indian J. Environ. Health* **2002**, *44*, 78–87.
36. Rao, M.; Parwate, A.; Bhole, A. Removal of Cr⁶⁺ and Ni²⁺ from aqueous solution using bagasse and fly ash. *Waste Manag.* **2002**, *22*, 821–830. [[CrossRef](#)]
37. Gupta, S.; Babu, B. Removal of toxic metal Cr (VI) from aqueous solutions using sawdust as adsorbent: Equilibrium, kinetics and regeneration studies. *Chem. Eng. J.* **2009**, *150*, 352–365. [[CrossRef](#)]
38. Gritti, F.; Guiochon, G. Adsorption mechanisms and effect of temperature in reversed-phase liquid chromatography. Meaning of the classical Van't Hoff plot in chromatography. *Anal. Chem.* **2006**, *78*, 4642–4653. [[CrossRef](#)]
39. Qiu, S.; Wu, L.; Pan, X.; Zhang, L.; Chen, H.; Gao, C. Preparation and properties of functionalized carbon nanotube/PSF blend ultrafiltration membranes. *J. Membr. Sci.* **2009**, *342*, 165–172. [[CrossRef](#)]
40. Kuppusamy, S.; Thavamani, P.; Megharaj, M.; Venkateswarlu, K.; Lee, Y.B.; Naidu, R. Potential of Melaleuca diosmifolia leaf as a low-cost adsorbent for hexavalent chromium removal from contaminated water bodies. *Process Saf. Environ. Prot.* **2016**, *100*, 173–182. [[CrossRef](#)]
41. Salman, S.M.; Ali, A.; Khan, B.; Iqbal, M.; Alamzeb, M. Thermodynamic and kinetic insights into plant-mediated detoxification of lead, cadmium, and chromium from aqueous solutions by chemically modified Salvia moorcroftiana leaves. *Environ. Sci. Pollut. Res.* **2019**, *26*, 14339–14349. [[CrossRef](#)]
42. Ponou, J.; Kim, J.; Wang, L.P.; Dodbiba, G.; Fujita, T. Sorption of Cr (VI) anions in aqueous solution using carbonized or dried pineapple leaves. *Chem. Eng. J.* **2011**, *172*, 906–913. [[CrossRef](#)]
43. Mondal, N.K.; Samanta, A.; Roy, P.; Das, B. Optimization study of adsorption parameters for removal of Cr (VI) using Magnolia leaf biomass by response surface methodology. *Sustain. Water Resour. Manag.* **2019**, *5*, 1627–1639. [[CrossRef](#)]
44. Rehman, R.; Anwar, J.; Mahmud, T.; Salman, M.; Saleem, M. Evaluation of batch biosorption of chromium (VI) from aqueous solution by chemically modified Polyalthialongifolia leaves. *J. Chem. Soc. Pak* **2011**, *33*, 846.